Typeset manuscript available here:
https://doi.org/10.1016/j.powtec.2016.11.051

Please cite as:
Jones, T.J., Russell, J.K., Lim, C.J., Ellis, N. and Grace, J.R., 2017. Pumice attrition in an air-jet. *Powder Technology*, *308*, pp.298-305.

Pumice attrition in an air-jet

T. J. Jones[1,2*], J.K. Russell[2], C.J. Lim[3], N. Ellis[3] and J.R. Grace[3]

[1] Department of Earth Sciences, Durham University, South Road, Durham, DH1 3LE, UK

[2] Department of Earth, Ocean & Atmospheric Sciences, University of British Columbia, Vancouver, British Columbia, V6T 1Z4, Canada

[3] Department of Chemical and Biological Engineering, University of British Columbia, Vancouver V6T 1Z3, Canada

Typeset manuscript available here:
https://doi.org/10.1016/j.powtec.2016.11.051

Abstract

We present the results from a series of jet-attrition experiments performed using a standard ASTM device (ASTM D5757-00) on naturally occurring ash-sized (< 2 mm) pumice, a product of explosive volcanic eruption comprising highly porous silicate glass. We investigate the effect of both feed grain size and attrition duration on the production of fines. We utilize a wet methodology for fines collection to ensure recovery of the total grain size distribution for each experimental run. The experiments convert a restricted size range of pumice particles to a bimodal population of parent and daughter particles. The bimodal distribution develops even after short (~15 mins) attrition times. With increased attrition time, the volume of daughter particles increases and the mode migrates to finer grain sizes. Jet attrition efficiency depends heavily on the particle size of the feed; our data show little attrition for a feed of 500 μm *vs*. highly efficient attrition for a 250 μm feed. Our rates of attrition for pumice are extremely high compared to rates recovered from experiments on limestone pellets. Our fines production data are well modeled by:

$$\frac{m_{fines}}{m_{bed}^{0}} = 0.291(1 - e^{-0.312t})$$

where m^{0}_{bed} is the initial mass of particles in the bed, t is in hours, and the two adjustable coefficients dictate the long time limiting behaviour (0.291) and rate at which the limit is reached (-0.312). This functional form provides more realistic limits in time while preserving a zero intercept and defining a plateau for long residence times.

Keywords: Pumice; attrition; milling; ash production; fines production model; ASTM D5757-00

Typeset manuscript available here:
https://doi.org/10.1016/j.powtec.2016.11.051

1. Introduction

Particle attrition is a process that operates in a diverse range of engineering and natural environments to cause particle size reduction, as well as, reshaping and resurfacing of particles. In the engineering sciences, particle attrition studies are commonly experimental in nature and concern the mechanisms, rates, and consequences of attrition in fluidized and conveyed systems. The experiments involve diverse materials such as: fluid cracking catalysts [1], limestone particles [2], and CO_2 sorbent pellets [3][4], tested under conditions relevant to the engineering environment. Attrition is also widespread in geological processes including sediment transport (e.g., stream beds, beach sand), volcanic eruption (e.g., xenolith milling), and glaciation (e.g., till deposits). There are, however, few experimental studies of attrition in geologically relevant systems or on geological materials. Exceptions include, but are not limited to: secondary fragmentation of crystal rich ash [5]; rounding of pumice clasts during transport in pyroclastic density currents [6]; wear of kimberlitic minerals [7–10]; milling of lithic material within volcanic conduits [11] and abrasion of geological materials by eolian action [12].

Pumice is a naturally occurring resource produced through explosive volcanic eruptions. It is commonly defined as a highly vesicular silicic to mafic glass foam, having a bulk density less than water (i.e. floatable) [13][14]. Pumice represents an interesting material because it has unique properties: high vesicularity, low density, and a contiguous glass (i.e. not crystalline) framework. This porous volcanic material is of interest to both engineering and geological sciences. Some existing uses of pumice in industry include: a natural pozzolan for cement [15]; abrasives in skin products and dentistry; water filtration [16]; as a chemical or catalyst carrier in fluidisation systems [17,18] and as an inert fluidising solid [19]. These latter applications are of particular relevance to this study; if pumice is to be used in a fluidised system it is important to understand how grain size may evolve with residence time in the fluidised apparatus. On its own, pumice has low strength due to its highly vesicular nature and is easily broken down by crushing and fracturing of the thin, typically interconnected, glass bubble walls. Its low density has made it an ideal aggregate in cement to reduce the density of concrete; it does so without reducing the strength of the concrete significantly.

Yet, despite its widespread industrial uses and its importance in geology, its susceptibility to attrition remains poorly known [20]. Pumice attrition has rarely been studied experimentally. Previous experimental work on pumice has shown the grain size reduction of pumice by ball milling [21–23] and the decrease in fines production with increased milling duration by rock tumbling [6,24]. These experiments inform on attrition processes typically involving continual particle-particle contact whereas air-jet experiments feature much shorter durations of particle-particle contact. A small amount of experimental work involving fluidization of pumice [25,26] has been done in volcanology with the aim of understanding: grain size distributions and sorting within natural deposits; the degree of particle segregation during flow; and elutriation of fine particles produced by attrition.

Here we present a suite of attrition experiments involving particles of pumice within an ASTM standard device providing a particle-laden jet. Our experiments are designed to further our understanding of how pumice (i.e. porous glassy material) undergoes grain size reduction in a gas jet and have relevance to fluidised beds using pumice as a catalyst support [27–29]. The experiments use well-characterized pumice particles having a known initial total grain size distributions (TGSD) and bed mass are subjected to jet attrition for fixed amounts of time. We then collect the experimental run-products and process them for their TGSD and use the data to establish rates/mechanisms for pumice attrition and the evolution of grain size with residence time.

2. Review of Attrition in a Gas Jet

Attrition processes comprise two primary mechanisms of particle size reduction: fragmentation and abrasion. Fragmentation refers to particle fracturing wherein the original particles (i.e. parent or mother particles), subjected to critical collisions are mechanically broken into smaller particles (i.e. daughter particles). Collisions causing fragmentation typically result from direct impact with other particles or a hard surface at, or above, a critical threshold velocity. Commonly the parent particle is fragmented into a number of smaller particles of similar size. Attrition by abrasion is a less energetic mechanism involving wearing or rounding the rough edges or asperities of mother and daughter particles via lower energy particle-particle impacts. Abrasion generates a significant number of very fine particles, leading to bimodal grain size distributions, and creates particles with smoother morphologies.

Several factors govern the mechanisms and efficiency of attrition in fluidized gas-solid systems. The environmental factors, or experimental controls, include residence time in the attrition jet, temperature, gas type, vessel pressure, bed load and gas velocity. The important material properties governing attrition include grain size, hardness or strength, density, particle shape and surface texture [1].

Gwyn [30] was one of the first to study and model the production of fines in a fluidized system by attrition. His attrition experiments showed the production of fines to vary non-linearly with time (*t*) and he modelled the fines production as:

$$\frac{m_{fines}}{m_{bed}^{0}} = K_a t^b \qquad [1]$$

where m_{fines} and $m^0{}_{bed}$ are the mass of fines and the initial bed particles, respectively [30]. The parameters K_a and b are constants determined by fitting Eq. 1 to experimental data. Commonly the experimental data show a dramatic and rapid decay in attrition rate after a brief period of *initial attrition* where the rough edges of the original particles are broken off to form smoother surfaces [30]. This empirical equation captures this behaviour well and the Gwyn model has been used extensively to describe many different experimental datasets. However, one recognized limitation of Eq. 1 is that it assumes that all collisions are below a threshold velocity that would cause particle fracturing, creating new rough fracture edges [4]. Subsequent extensions of the Gwyn model focused on the three main areas of fluidized systems where attrition can occur: jet attrition [31]; bed and bubble attrition [32] and cyclone attrition [33].

In this study, we focus on jet attrition, the dominant mechanism operating within our experimental set-up (Figure 1; [2,4,34]). When jet attrition is the dominant process, the mass of fines produced through time can be modeled as:

Typeset manuscript available here:
https://doi.org/10.1016/j.powtec.2016.11.051

$$m_{jetfines} = C_{jet} d_{pb} n_{or} \rho_g d_{or}^2 u_{or}^2 \qquad [2]$$

where C_{jet} is a fitted constant, d_{pb} is the bed particle diameter, n_{or} is the number of orifices, ρ_g is the fluidizing gas density, d_{or} is the orifice diameter and u_{or} is the gas velocity at the orifice. Alternatively, the attrition rate can be modeled with the mean particle diameter ($\bar{d}$). This is less common, due to the extra work needed to characterize the particle size distribution (PSD), however it enables a complete understanding of the attrition processes (abrasion vs. fragmentation) operating.

3. Methodology

3.1 Pumice samples from Mount Meager, British Columbia

The Mount Meager volcanic complex is a calc-alkaline stratovolcano complex situated approximately 150 km north of the city of Vancouver, in southwestern British Columbia and belongs to the northernmost extension of the Cascade Volcanic Arc [35]. The most recent eruption of the Mount Meager is dated to 2360 BP [36] and produced explosive and effusive dacite volcanic deposits including: pyroclastic fall deposits, pyroclastic flow deposits, and lava [37]. For this study, blocks (> 10 cm) of pumice were collected from proximal to medial outcroppings of the pyroclastic fall deposit. The fallout deposit (Pebble Creek Formation of [35]) varies in thickness from 1 m to > 60 m near the volcanic vent, contains > 90% white to grey-white pumice clasts and is matrix free [35]. Pumice blocks from the fallout deposit have total porosity ranging from 60 - 75% [38], a skeletal (bubble free) density of 2255 kgm^{-3} [39], a crystallinity ranging from 14 to 8% [40].

The pumice blocks were crushed and then manually dry sieved using a standard stack of Tyler sieves. The grain size fractions caught in the 500 μm and 250 μm mesh screens were divided into 20 g aliquots and stored in an airtight container ready for the experiments. Throughout this paper we refer to each grain size fraction by its catching sieve. For example, the 250 μm input material was caught in the 250 mesh and therefore contained fragments >250 μm but <500 μm.

3.2 Jet attrition rig

Typeset manuscript available here:
https://doi.org/10.1016/j.powtec.2016.11.051

All experiments (Table 1) were performed at atmospheric temperature and pressure in a jet attrition rig (Figure 1) with dry air fed at 10 ±0.5 L min^{-1}, based upon the ASTM D5757-00 method [4,42]. This experimental rig consists of a flat, horizontal basal distributor plate with three orifices 0.397 mm in diameter on which the initial sample is loaded (Figure 1). Directly above the distributor a 710 mm long, 35 mm internal diameter stainless steel attrition tube is connected. Then the settling chamber is connected to the top of the attrition tube; it is wider in diameter (110 mm in the center) allowing for large particle settling and return to the attrition tube. The upper cone of the attrition chamber is connected to a fines collection bin. To enable gas to fully flow through the system, a gas exit pipe is connected to a ceramic filter within the fines collector bin. This ceramic filter has holes ~0.1 μm in diameter to prevent the fines from escaping.

In this study we investigate the effects of variable attrition duration and feed size on the same material: naturally occurring pumice from Mount Meager. For each experiment the distributor plate, gas feed and attrition tube were connected, after which a 20 g sample of either 250 μm or 500 μm Mt. Meager pumice was introduced. Specifically, the sieved pumice sample was poured down the attrition tube to rest on the distributor plate after which the settling chamber and fines collector were connected. In-line building dry air was connected via a calibrated rotameter and increased to a flow rate of 10 liters per minute whilst checking for leaks. Providing the system was free of gas leakage, the experiment was left to run for the full prescribed duration. We performed experiments for 0.25, 0.5, 0.75, 1, 2, 3, 5, 16 and 24 hours for the 250 μm input material and for 16 and 24 hours for the 500 μm input grain size fraction. At the end of each experiment, the gas was switched off and the sample material was left to settle for at least 1 hour after gently knocking the apparatus to loosen adhering fine particles.

The product particles from each experiment were collected in three stages. Firstly, the fines collector (Figure 1) was removed and its contents (ultra-fine ~ < 4 μm particles) were brushed into a collection pot for post-experiment analysis. Secondly, the ‘empty’ fines collector, connecting pipes and the settling chamber were rinsed at least twice with deionised water over a 63 μm sieve to remove any remaining fines adhering to the walls of the apparatus. We then removed the distributor plate within a sample collection bag to recover all of this material, making sure to brush all of the bolts/washers to recover the entire sample. Lastly, the attrition tube was flushed again with deionised water over a 63 μm sieve. This sieve was then dried in an oven and added to all the dry recovered material. We developed and recommend this "wet" collection method and cleaning procedure of the jet attrition rig because it ensures accurate and complete recovery of all particles, especially the finest material, produced in the attrition experiment. Brushing, for example, will often lose the finest particles that are inevitably lofted into the air. By flushing the system with water the particles become entrained and suspended and can be easily collected in the wash. Furthermore, this collection method allows for a more accurate estimate of the mass fraction of total fines (i.e. 63 μm) and the measurement of the total grain size distribution curves (TGSD) for each experiment. TGSD curves can be analysed for information on the relative proportion of parent material and daughter products, the full size range of fines produced and the statistical distribution of products (e.g. log-normal). However, we note that this wet collection method may not be suitable for all materials and may lead to unreliable results if particles absorb large amounts of water (e.g. clays) or undergo chemical reaction when wet.

3.3 Post-attrition sample characterisation

Given the electrostatic properties of fine pumice particles and the fine grain size of the experimental products, sieving can lead to large errors due to particle aggregation. Therefore, the entire recovered sample for each experiment was added to a small (~250ml) flask of deionised water. Each flask contained all of the recovered particles from a single attrition experiments and were subsequently measured using a Malvern Mastersizer 2000 with the hydro 2000Mu water dispersion module attached. This laser particle analyser is capable of measuring particles ranging from 0.02 to 2000 μm in size. Using a pump speed of 1900 rpm an aliquot of the attrition sample was added to the dispersion module and measured three times. An ultrasonic pulse was applied to the sample for 2 s before the measurement to prevent particles from aggregating in the water suspension. For each experimental product three separate aliquots were taken, each measured three times; the results presented here therefore represent averages of nine measurements. No merging of datasets was required as the mastersizer analysed the complete total grain size distribution in a single measurement run.

4. Results and Analysis

4.1 ASTM fines collector

Results of the nine experiments using the 250 μm grain size pumice show rapid and pronounced attrition (Figure 2). The rate and extent of attrition are summarized in Figure 2 as, both, the production of fines and the reduction in grain size of the starting material with the duration of the attrition experiment. The 250 μm starting material reduces from 20 g to 6.1g in just 15 min (represented by open circles in Figure 2). In a similar manner the mass of material ~ < 4 μm collected in the fines collection bin (solid triangles) increases exponentially with increased attrition duration before reaching a plateau at ~ 6 g.

4.2 Air Jet Index

The experimental conditions and the materials used in our experiments do not exactly match previous experimental studies. There are two critical differences, firstly, we use a 20 g bed load rather than the conventional ASTM 50 g. Secondly, we use a wet collection method to recover the total grain size distributions, not just those retained in the fines collector. To facilitate comparison of our experimental data set to results from previous studies of particle attrition in a gas jet, we have calculated a modified Air Jet Index (AJI), defined as:

$$AJI = \frac{Mass\ of\ fines\ in\ collector}{Initial\ input\ mass} \times 100\% \qquad [3]$$

We express this parameter as 'modified' because the original AJI only considered material after a standard 5 hour ASTM experiment. We include a 5 hour experiment in order to match standard ASTM operating procedures but we have also calculated the parameter for the 8 other attrition durations (Table 2) to illustrate the transient evolution of the AJI. We compare our results to those for limestone particles intended for CO_2 capture in fluidized systems and considered to experience substantial attrition [4]. The limestone particles had a mean particle diameter of 1000 μm and were fluidized with humid air (10 L min^{-1}) at 20±3°C. Figure 3 shows that the pumice is much more susceptible to attrition than limestone under the same conditions; on the scale shown limestone produces minimal fines. For a conventional attrition duration of 5 h, limestone has an AJI of 0.2% whereas Mt Meager pumice has an AJI of 20.2%. For pumice it is clear that the modified AJI increases exponentially with attrition duration. This exponential increase in AJI has also been observed for other catalyst particles such as methanol to olefins (e.g., [43]). Hao et al., [43] also show that in addition to mechanical stress, thermal stresses may also influence the attrition of particles. To investigate this on pumice further experiments should be performed at evaluated temperature.

4.3 Total grain size distributions

Our procedure for collecting product particles from the experimental apparatus ensures that we were able to recover the entire experimental sample. Thus, in addition to measuring the total mass of the material that reached the fines collector after each experiment (Figures 2 and 3), we also measure the full grain size distribution of the run product for each attrition experiment. This enables us to describe how the grain or fragment size distribution changed with increasing attrition time (Figure 4). To illustrate the increased wealth of information derived from our sample collection procedure, we have calculated the maximum particle diameter able to enter the fines collector. This is the mass of sample expected to be recorded using the standard ASTM D5757-00 methodology. Our calculation is based on a Stokes law settling velocity of spherical particles against a 0.0175 ms^{-1} upward superficial velocity of gas within the settling chamber (Figure 1). Using with a skeletal (bubble free) density of 2255 kgm^{-3} [39] this gives a maximum particle diameter of 4.2 μm able to enter the fines collection bin.

The product particles derived from experiments using the 250 μm grain size initial material show a bimodal total GSD. They comprise a coarse peak that falls within the input size range (250 < d (μm) <500) and a fine peak that migrates to finer grain sizes with increased attrition. Finally, considering the material entering the fines collector (left of the dashed line), increasing the attrition time increased the volume of fines (area under the curve), confirming our results in Figure 2. It is clear that this metric (i.e. mass collected in fines collector) is useful as a monitor of attrition efficiency and rates. However, several other features relevant to understanding the mechanisms and rates of particle attrition are missed. Such features include the characteristic fragment size and the evolution of the parent and daughter subpopulations. Recovering a total GSD allows us to describe any bimodality in the data and the relative change in peak position. To illustrate this benefit, we now discuss some additional interpretations that become available from our TGSD vs. fines collection dataset.

Figure 4 provides a summary of the grain size distributions of all the experimental run products produced from an initial unimodal distribution between limits of 500 μm and 250 μm. It is clear that all experimental products show a bimodal distribution even after short residence times (i.e. 15 min). The bimodal distribution developed during attrition is comprised of a coarser material peak (399-283 μm) and a peak of finer material (40-14 μm). We suggest that the development of the bimodal distribution is a result of attrition involving, both, the fragmentation and abrasion of larger particles to make new smaller particles. Furthermore, the bimodal distributions are dynamic in that, both, the positions of the two peaks and their relative magnitudes change systematically with time. This shift represents an evolving population of both parent and daughter particles as they are subject to increased durations of attrition. This detailed analysis of grain size characteristics is only possible when a TGSD is collected as outlined.

We interpret the coarse and fine peaks as representing a residual population of the initial particles that are being attrited to produce smaller daughter fragments. The covariance between the coarse and fine peaks strongly supports the concept that these two populations are parent and daughter particles, respectively (Figure 5a). The parent peak can be described by its grain size (F_P) and magnitude (P); similarly the daughter peak can be located at grain size F_D with height D. The location of the parent particle peak shows no systematic trend with attrition time (Figure 5b); the distribution shown is likely to reflect the variability in feed material falling between the 500μm and 250μm sieves. Except for the 5-hour experiment, we observe the location of the daughter fragment peak shifting to smaller grain sizes with attrition duration (Figure 5c). At significantly longer attrition times (16 and 24 h), the size of the daughter products became stable, remaining at ~ 14 μm. This systematic shift in

Typeset manuscript available here:
https://doi.org/10.1016/j.powtec.2016.11.051

the modal daughter size represents continued abrasion that continually removes surface irregularities within this sub-population. Lastly, we are able to quantify the range in relative magnitude between the parent particles and the daughter products (Figure 5d). This is expressed as the fraction P/D; higher values indicate a greater number of parent particles remaining. An exponential decay of parent particles occurs with increased attrition time. The daughter particle population becomes larger than the input feed within 1 hour, again suggesting that the majority of attrition occurs within the first hour for all the 250 µm experiments.

4.4 Changing input grain size

In all experiments using a 250 µm feeding grain size we observed a rapid production of fines (Figures 2-5). However, in the experiments using a 500 µm input grain size we observed very different results – fines production was inhibited. For comparison we present two 24 hour experiments, one using an input grain size of 250 µm and the other a 500 µm input, represented by the light and dark grey bars in Figure 6 respectively. For the 500 µm feed experiment 92.5% of the material remained in the starting size bin, whereas for the 250 µm feed only 8.4% of the material remained in the starting grain size bin. For this smaller feed material, grain size reduction was efficient and reduced large proportions of material (36.4%) to diameters <63 µm. We observe that in comparison the 500 µm input material is extremely ineffective at producing fines <250 µm in diameter. From previous work on the suspension of pumice particles we know that the minimum velocity to keep 500 µm and 250 µm in suspensions is ~10^{-2} ms^{-1} [44]. Comparing this with the reported superficial gas velocity within the column/attrition tube (0.173 ms^{-1}) [45] supports our conclusion that all material is capable of being suspended by the gas jet.

In our experiments we suggest that limited fine production for the 500 µm feed is due to the relative number of particles suspended by the air jet and therefore able to partake in attrition processes (Figure 7). By continuity, the mass flow of particles (m_p) entrained in the three jets can be approximated by:

Typeset manuscript available here:
https://doi.org/10.1016/j.powtec.2016.11.051

$$m_p = \rho_p U_p (1-\phi)\frac{\pi}{4} D_c^2 \qquad [4]$$

where D_c is the internal diameter of the attrition tube, ρ_p is the particle density, ϕ is the measured void fraction (~0.47) and U_p is the (downwards) particle velocity (~5 mm s^{-1}) observed at the smooth wall of a transparent attrition tube. The mass flow rate was converted into an entrainment rate (i.e. number of particles entrained into the jets per second) by assuming spherical particles having grain sizes (750 and 375 µm) defined by the median size between pairs of screening sieves. We found that for the coarse feed size the number of particles entrained was 29 s^{-1}, whereas for the finer feed it was 231 s^{-1}. The number of suspended coarse particles may be further reduced if they rest far away from the gas jet on the distributer plate where gas velocities are not sufficient enough to lift the particles [44]. By halving the input feed size the number of particles in the jets increases by an order of magnitude. We suggest that such a high particle concentration in the jet promotes attrition because the chance of successful collisions is high.

5. Attrition Model

Our experimental results clearly demonstrate the extreme vulnerability of pumice particles to mechanical attrition. The rate of production of fines during attrition is exponential and can be described by the Gwyn model (Eq. 1; Table 2). To a first order the Gwyn model with best-fit parameters K_a= 0.09402 hrs^{-b} and b = 0.3901 fits our data well (Fig. 7a). The Gwyn model assumes that particle attrition is achieved solely through abrasion and that fragmentation does not occur. In our experiments, analysis of our TGSD curves (Figures 4 and 5) strongly suggests that parent particles are fragmented to produce daughter particles. Both these parent and daughter particles are also abraded (surface chips removed) during residency in the experiment.

The Gwyn model can reproduce our experimental data set (Fig. 7a) reasonably well, but there are two ways in which a better functional form is warranted. Firstly, the Gwyn model is intended to capture fines production due to abrasion, whilst our experiments indicate both fragmentation and abrasion. Secondly, the function implies no limit to fines production over longer high residence times;

the function continues to rise, becoming aphysical when it exceeds 1. Lastly, the form of the best fit Gwyn function has difficulty in reproducing data over both short and long residence times (Fig. 7b,c). To address these deficiencies, we have adopted a two-parameter model that obeys both the zero (no attrition at time zero) and infinite time limits:

$$\frac{m_{fines}}{m_{bed}^{0}} = 0.291(1 - e^{-0.312t}) \qquad [5]$$

where 0.291 is a constant that represents the amount of fines produced at long attrition durations and the exponent (-0.321) dictates how rapidly that limit is approached. Our model fit is shown in Figure 7b, compared to the Gwyn model (Equation 1; dashed line in Figure 7b). Our attrition model also fits the experimental data well even at short residence times (Figure 7c).

In Figure 2 we showed that the attrition can be ascribed to two stages, described by previous workers as a period of initial attrition followed by a longer period of stable attrition [2]. For the 250 μm feed pumice, the initial stage spanned an hour after which the attrition rate decreased as the system achieved a stable state at longer (> 1 h) residence times. We suggest that these high rates of initial attrition occur by exploiting naturally occurring defects in the pumice. Being a highly vesicular material, the interstitial glass and microcrystalline matrix form a delicate network, connected in places by thin bubble walls. In addition, the particle exterior is initially highly irregular. It is likely that only small differential velocities are required to chip and break this irregular particle exterior connected by delicate bubble walls (Figure 8). The chance for a collision to be successful in abrading or fragmenting the parent particle is high during this initial attrition phase. Lastly, following the period of initial attrition, the rate decays and becomes relatively stable. Further attrition is inhibited because all irregularities on the particle surface have been removed. For the 250 μm feed experiments at relatively long residence times (16 and 24 h) the mean size of the daughter fragments does not decrease. We suggest that this size (14.2 μm) marks a minimum stable pumice fragment grain size achievable by these standard ASTM conditions.

The processes we have described in our attrition model for the porous volcanic material have large implications for both the engineering and geological sciences. Firstly, in engineering the naturally occurring resource, pumice, is often used to carry a catalyst or to act as in inert material in fluidised beds [e.g., 15,16]. To use this material effectively in fluidised systems the role of attrition must be considered. The findings presented here will enable users to predict the rate of attrition and fines generation and therefore its stability in a fluidised system. Secondly, in volcanology pumice is commonly transported in a gas suspension during a volcanic eruption. For example, previous work has shown secondary fragmentation and attrition to occur within the conduit during the ascent of a gas particle mixture [e.g., 10,19]. Our experiments and quantitative analysis have strong implications for the rates of attrition and grain size reduction during this style of volcanic transport.

6. Summary

In this paper we adopted the methodology of the ASTM D5757-00 standard attrition test, with particular emphasis on the recovery of an entire grain size distribution from each experiment. By thorough water flush collection, we were able to analyze the total grain size distribution produced, rather than just the mass recovered in the fines collection bin. This technique allows for further insights into the attrition method operating (abrasion or fragmentation). We found that for Mt Meager pumice under ASTM test conditions (room temperature, 10 L min^{-1} dry air) attrition mainly occurred through abrasion. Furthermore, we investigated how the parent and daughter population changed in mean grain size and magnitude with increased residence time. We found that the parent size remained within its original limits. However, the magnitude/volume of parent material decreased with increased attrition. The daughter fragmentation population increased in volume and migrated to finer mean grain sizes with increased attrition. We have also shown that the amount of suspended particles in the jet is a critical metric for attrition (Figure 8). Sufficient particle concentrations must be suspended for attrition to occur leading to fines preserved in the collection box. If the particle concentrations in the jet are not high enough no ultra-fine material will be produced, and all grain modifications remain on the distributor plate. Lastly, we present an alterative fines production model to that of Gwyn (1969), incorporating an infinite time condition where fines production ceases. This study has presented the first dataset on Mt. Meager pumice in a standard air-jet attrition device (ASTM D5757-00); our results quantify the extreme susceptibility for pumice to undergo attrition in a fluidized environment.

Furthermore, this study has broad reaching implications outside of engineering; the attrition of pumice has particular relevance to the volcanological sciences. For example the attrition of pumice to produce fine ash impacts the characteristics of tephra deposits [5]; aviation hazard [46] and plume dynamics [20].

Acknowledgements

JKR is supported by the Natural Sciences and Engineering Research Council of Canada through the Discovery Grants and Discovery Accelerator Supplements programs. TJJ was funded by NERC NE/L0025901, part of the IAPETUS doctoral training partnership.

References:

[1] W.L. Forsythe, W.R. Hertwig, Attrition characteristics of fluid cracking catalysts, Ind. Eng. Chem. 41 (1949) 1200–1206.

[2] G. Xiao, J.R. Grace, C.J. Lim, Attrition characteristics and mechanisms for limestone particles in an air-jet apparatus, Powder Technol. 207 (2011) 183–191.

[3] Z. Sun, M. Xiao, S. Wang, D. Han, S. Song, G. Chenb, Y. Meng, Materials Chemistry A, (2014).

[4] A. Knight, N. Ellis, J.R. Grace, C.J. Lim, CO 2 sorbent attrition testing for fluidized bed systems, Powder Technol. 266 (2014) 412–423.

[5] T.J. Jones, K. McNamara, J. Eychenne, A.C. Rust, K. V Cashman, B. Scheu, R. Edwards, Primary and secondary fragmentation of crystal bearing intermediate magma, J. Volcanol. Geotherm. Res. (2016).

[6] M. Manga, A. Patel, J. Dufek, Rounding of pumice clasts during transport: field measurements and laboratory studies, Bull. Volcanol. 73 (2011) 321–333.

[7] T.E. McCandless, Kimberlite xenocryst wear in high-energy fluvial systems: Experimental studies, J. Geochemical Explor. 37 (1990) 323–331.

[8] T.J. Jones, J.K. Russell, L.A. Porritt, R.J. Brown, Morphology and surface features of olivine in kimberlite: implications for ascent processes, Solid Earth. 5 (2014) 313.

[9] V.P. Afanas' ev, E.I. Nikolenko, N.S. Tychkov, A.T. Titov, A. V Tolstov, V.P. Kornilova, N. V Sobolev, Mechanical abrasion of kimberlite indicator minerals: experimental investigations, Russ. Geol. Geophys. 49 (2008) 91–97.

[10] R.C. Brett, J.K. Russell, G.D.M. Andrews, T.J. Jones, The ascent of kimberlite: Insights from olivine, Earth Planet. Sci. Lett. 424 (2015) 119–131. doi:http://dx.doi.org/10.1016/j.epsl.2015.05.024.

[11] M.E. Campbell, J.K. Russell, L.A. Porritt, Thermomechanical milling of accessory lithics in volcanic conduits, Earth Planet. Sci. Lett. 377 (2013) 276–286.

Typeset manuscript available here:
https://doi.org/10.1016/j.powtec.2016.11.051

[12] P.H. Kuenen, Experimental abrasion 4: eolian action, J. Geol. (1960) 427–449.

[13] A.G. Whitham, R.S.J. Sparks, Pumice, Bull. Volcanol. 48 (1986) 209–223. doi:10.1007/BF01087675.

[14] R. V Fisher, H.U. Schmincke, Pyroclastic rocks, 472 pp, Springer, Berlin, Doi. 10 (1984) 973–978.

[15] S. Seraj, R. Cano, S. Liu, D. Whitney, D. Fowler, R. Ferron, J. Zhu, M. Juenger, Evaluating the Performance of Alternative Supplementary Cementing Material in Concrete, 2014.

[16] S. Karthikeyan, C. Anandan, J. Subramanian, G. Sekaran, Characterization of iron impregnated polyacrylamide catalyst and its application to the treatment of municipal wastewater, RSC Adv. 3 (2013) 15044–15057.

[17] D. Dodman, K. Pearson, J. Woolley, Catalytic carbonylation of aromatic nitroso compounds to prepare corresponding isocyanates, (1973).

[18] R. Andrzej, R.H. Lister, Vanadium pentoxide potassium pyrosulfate catalyst and method of preparation thereof, (1965).

[19] M.G. Rasul, Fluidization Characteristics of Bagasse in a Gas-Fluidized Bed, Part. Part. Syst. Charact. 15 (1998) 243–247.

[20] J. Dufek, M. Manga, A. Patel, Granular disruption during explosive volcanic eruptions, Nat. Geosci. 5 (2012) 561–564.

[21] V. Deniz, T. Onur, Investigation of the breakage kinetics of pumice samples as dependent on powder filling in a ball mill, Int. J. Miner. Process. 67 (2002) 71–78.

[22] V. Deniz, Investigation of breakage behaviour of two different pumice stones, Eur. J. Miner. Process. Environ. Prot. 4 (2004) 162–167.

[23] V. Deniz, Breakage properties of porous materials by ball milling, in: 19th Int. Min. Congr. Fair Turkey, IMCET2005, Izmir, Turkey, 2005: pp. 207–211.

[24] U. Kueppers, C. Putz, O. Spieler, D.B. Dingwell, Abrasion in pyroclastic density currents: insights from tumbling experiments, Phys. Chem. Earth, Parts A/B/C. 45 (2012) 33–39.

[25] C.J.N. Wilson, The role of fluidization in the emplacement of pyroclastic claws: An experimental approach, J. Volcanol. Geotherm. Res. 8 (1980) 231–249. doi:http://dx.doi.org/10.1016/0377-0273(80)90106-7.

[26] T. Gravina, L. Lirer, A. Marzocchella, P. Petrosino, P. Salatino, Fluidization and attrition of pyroclastic granular solids, J. Volcanol. Geotherm. Res. 138 (2004) 27–42. doi:http://dx.doi.org/10.1016/j.jvolgeores.2004.06.005.

[27] R.J. Blake, G.W. Roy, Oxychlorination of saturated and unsaturated hydrocarbons in the presence of a fluidized catalyst containing lanthanum and didymium, (1972).

[28] S.K. Bhattacharyya, R. Krishnamurthy, Catalytic vapour-phase oxidation of xylenes in fluidised bed, J. Appl. Chem. 13 (1963) 547–552.

[29] M.D. Balaguer, M.T. Vicent, J.M. Paris, Utilisation of pumice stone as support for the anaerobic treatment of vinasse with a fluidized bed reactor, Environ. Technol. 12 (1991) 1167–1173.

[30] J.E. Gwyn, On the particle size distribution function and the attrition of cracking catalysts,

AIChE J. 15 (1969) 35–39.

[31] J. Werther, W. Xi, Jet attrition of catalyst particles in gas fluidized beds, Powder Technol. 76 (1993) 39–46.

[32] Y.-C. Ray, T.-S. Jiang, C.Y. Wen, Particle attrition phenomena in a fluidized bed, Powder Technol. 49 (1987) 193–206.

[33] J. Reppenhagen, J. Werther, Catalyst attrition in cyclones, Powder Technol. 113 (2000) 55–69.

[34] G. Xiao, J.R. Grace, C.J. Lim, Evolution of Limestone Particle Size Distribution in an Air-Jet Attrition Apparatus, Ind. Eng. Chem. Res. 53 (2014) 15845–15851.

[35] C.J. Hickson, J.K. Russell, M. V Stasiuk, Volcanology of the 2350 BP eruption of Mount Meager volcanic complex, British Columbia, Canada: implications for hazards from eruptions in topographically complex terrain, Bull. Volcanol. 60 (1999) 489–507.

[36] J.J. Clague, S.G. Evans, V.N. Rampton, G.J. Woodsworth, Improved age estimates for the White River and Bridge River tephras, western Canada, Can. J. Earth Sci. 32 (1995) 1172–1179.

[37] G.D.M. Andrews, J.K. Russell, M.L. Stewart, The history and dynamics of a welded pyroclastic dam and its failure, Bull. Volcanol. 76 (2014) 1–16.

[38] D. Gainer, Porosity-viscosity relationships during compaction of pumice, article, University of British Columbia, 2013.

[39] S. Kolzenburg, J.K. Russell, Welding of pyroclastic conduit infill: A mechanism for cyclical explosive eruptions, J. Geophys. Res. Solid Earth. 119 (2014) 5305–5323.

[40] J. Welles, Effects of porosity on compressional wave velocities in volcanic rocks, University of British Columbia, 2012.

[41] B.M. Kennedy, F.B. Wadsworth, J. Vasseur, C. Ian Schipper, A. Mark Jellinek, F.W. von Aulock, K.-U. Hess, J. Kelly Russell, Y. Lavallée, A.R.L. Nichols, D.B. Dingwell, Surface tension driven processes densify and retain permeability in magma and lava, 2016. doi:10.1016/j.epsl.2015.10.031.

[42] Z. Chen, C.J. Lim, J.R. Grace, Study of limestone particle impact attrition, Chem. Eng. Sci. 62 (2007) 867–877.

[43] J. Hao, Y. Zhao, M. Ye, Z. Liu, Attrition of methanol to olefins catalyst with high-velocity air jets at elevated temperature, Adv. Powder Technol. 26 (2015) 734–741. doi:10.1016/j.apt.2015.03.010.

[44] G.A. Douillet, K.R. Rasmussen, U. Kueppers, D. Lo Castro, J.P. Merrison, J.J. Iversen, D.B. Dingwell, Saltation threshold for pyroclasts at various bedslopes: Wind tunnel measurements, J. Volcanol. Geotherm. Res. 278 (2014) 14–24.

[45] A. Knight, Sorbent attrition in fluidized carbon dioxide capture systems, (2013).

[46] U. Kueppers, C. Cimarelli, K.-U. Hess, J. Taddeucci, F.B. Wadsworth, D.B. Dingwell, The thermal stability of Eyjafjallajökull ash versus turbine ingestion test sands, J. Appl. Volcanol. 3 (2014) 4.

[47] M.E. Campbell, L. Porritt, J.K. Russell, Forensic recovery of transient eruption parameters for the 2360BP fall deposit, Mount Meager, British Columbia, J. Volcanol. Geotherm. Res. 312 (2016) 11–25.

Typeset manuscript available here:
https://doi.org/10.1016/j.powtec.2016.11.051

Figure Captions

Figure 1. Schematic representation of standard ASTM experimental apparatus (ASTM D5757-00) used for jet attrition experiments (modified from [4]).

Figure 2. Summary of experimental results expressed in terms of masses of residual particles ~ 250 μm in diameter (solid triangles) and masses of < 250 μm diameter fine particles from the collector (open circles) as a function of time: (A) Experimental data plotted over full experimental time scale (25 h); grey shaded vertical box denotes area enlarged and shown in (B) over a shorter (1 h) timescale.

Figure 3. Variations in Attrition Jet Index (AJI; [4]) with total residence time. Experimental data on pumice attrition from this work (grey squares) are compared to published data on limestone particles (black squares; Knight et al. [4]).

Figure 4. Results of attrition experiments expressed as total grain size distribution curves comprising integrated size fractions as volume % measured by conventional sieving and by laser diffraction particle size analysis. The grain size distribution curves comprise two peaks which vary systematically in position and amplitude as a function of total attrition time).

Figure 5. Detailed analysis of total grain size distribution datasets (cf. Fig. 4). (A) Schematic diagram defining metrics used to characterize individual grain size (vol. %) distribution curves including: i) positions of two prominent peaks corresponding to the original (parental) mean particle size (F_P) and mean size of daughter particles (F_D); ii) respective amplitudes P and D. (B) F_P plotted against total attrition time. (C) F_D plotted against total attrition time. (D) Ratio of parent to daughter peak heights (P/D) plotted against experimental residence time.

Figure 6. Data collected from attrition experiments (Table 1) designed to explore the effects of initial particle size on rates of jet attrition. Results of two experiments on pumice particles having mean grain sizes ~500 and ~250 um expressed as the mass % recovered in each size interval after 24 h of attrition. The 24 h experiment caused little attrition of the 500 µm sample because of less efficient entrainment of particles into the jet.

Figure 7. Data from attrition experiments summarized as mass of fine (< 4 µm) particles produced by attrition normalized by the initial mass of particles in the bed (> 4 µm). **(a)** Experimental data (solid circles) are compared to best-fit curve based on equation proposed by Gwyn (1969). **(b)** The experimental data (solid circles) compared to best fit curve for Eq. 4 which offers a better functional form that preserves a zero intercept and rises to a fixed plateau. **(c)** Comparison of model curves to experimental data over restricted interval of 0-10 h (grey shaded time interval in b).

Figure 8. Schematic diagrams of particle movement and entrainment within ASTM jet attrition device. **(a)** Idealized jet showing regions of entrainment and ideal particle trajectories (modified from [2]). **(b)** Jet-particle interaction portrayed schematically for feed of >500 µm particles showing poor particle entrainment (~29 particles/s) resulting in low concentrations of particles in the jet, reducing opportunities for particle-particle collisions. **(c)** Jet-particle interaction for feed of >250 µm particles

representing more efficient particle entrainment by the jet (~231 particles/s) leading to a particle-laden jet with many successful attrition-producing collisions.

Table 1. Summary of experiments conducted on pumice from Mount Meager (MMP;[47]). For all experiments dry air was fed at 10 ±0.5 L min^{-1} and 20 ±1°C.

Table 2. Mass of fine particles (~ < 4 μm) collected from Fines Collection box (Fig. 1) for attrition experiments with a feed of 250 μm pumice particles.

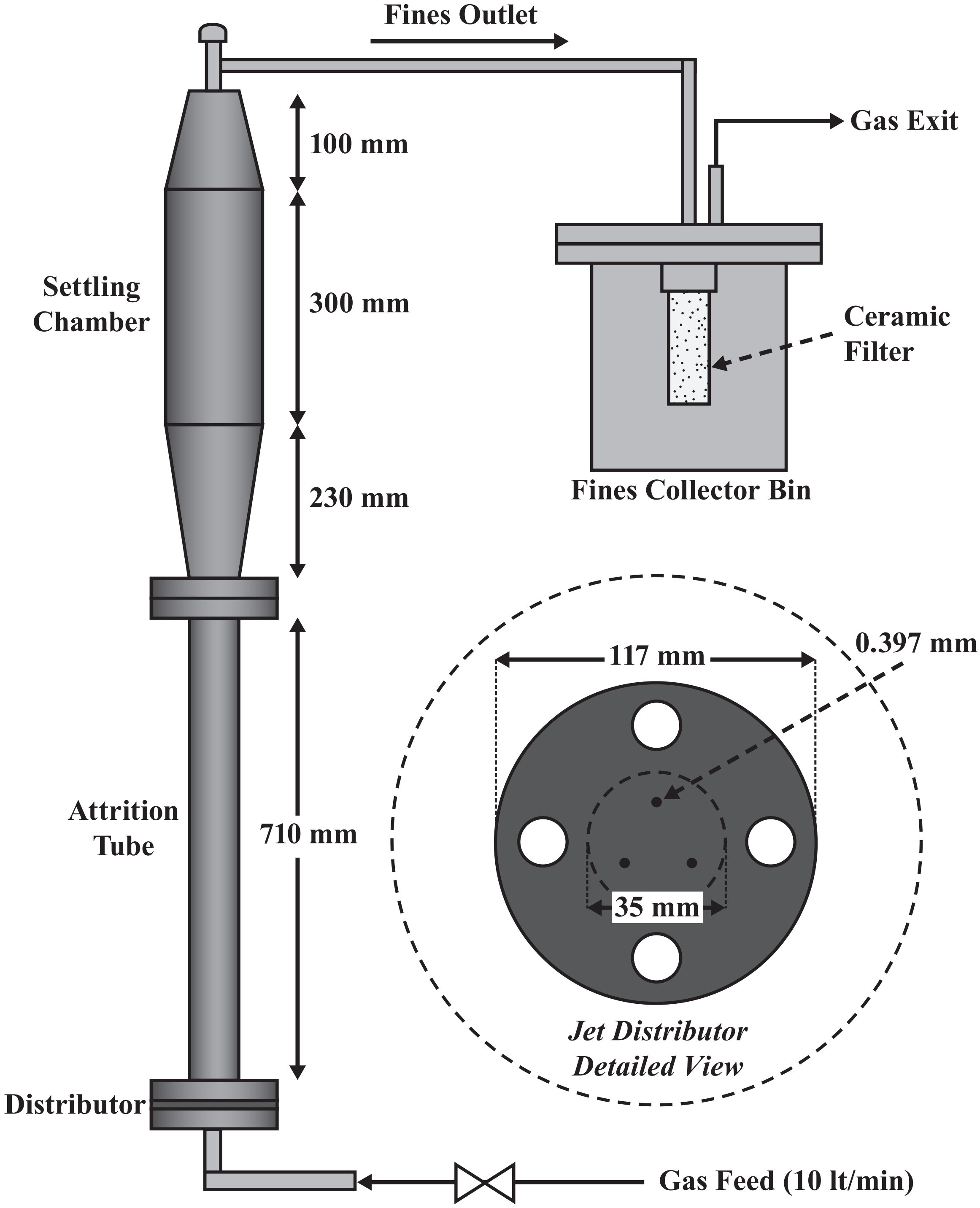

Figure 1: Jones et al., (in prep. for powder tech.)

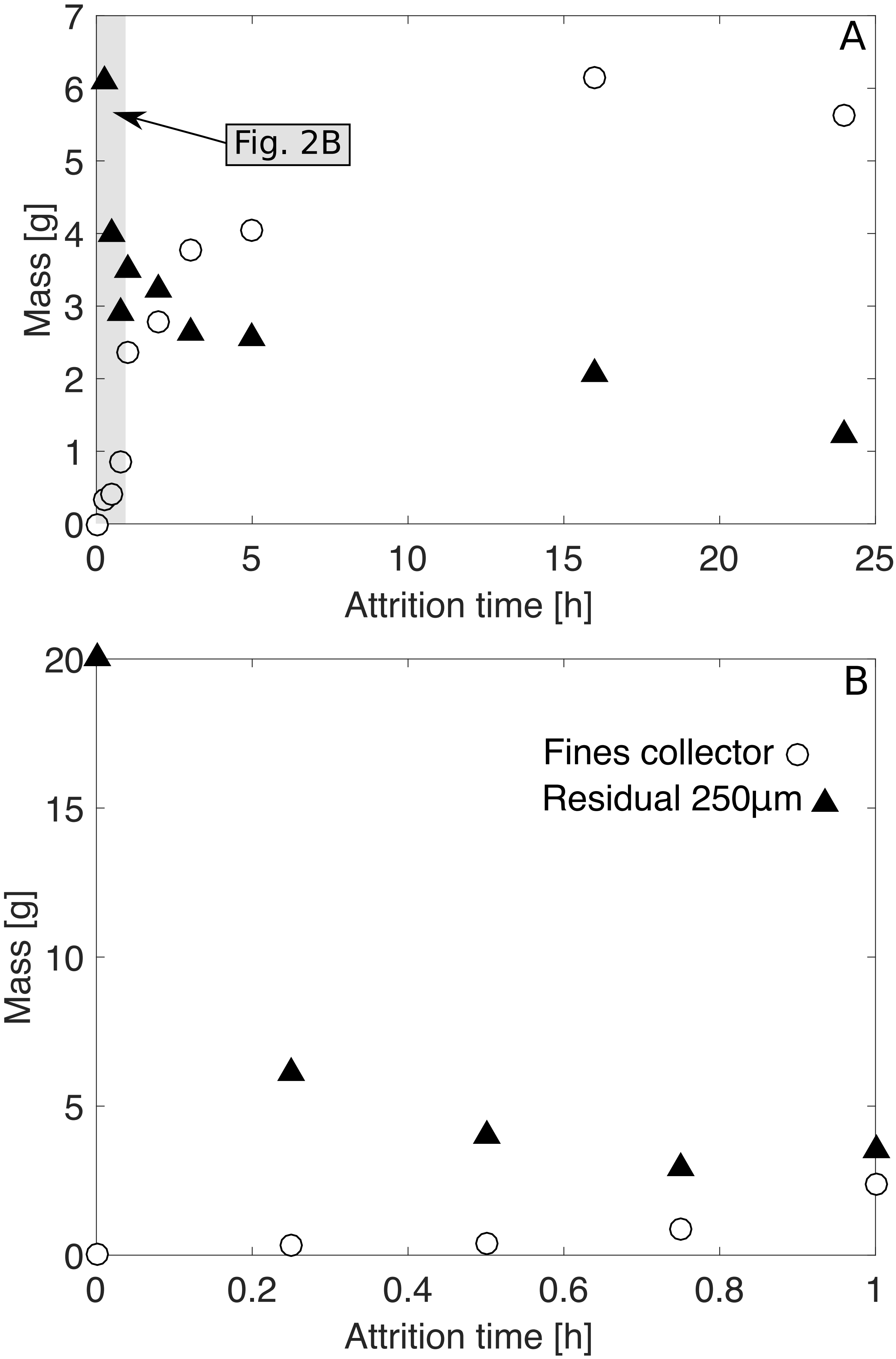

Figure 2: Jones et al., (in prep. for Powder Tech.)

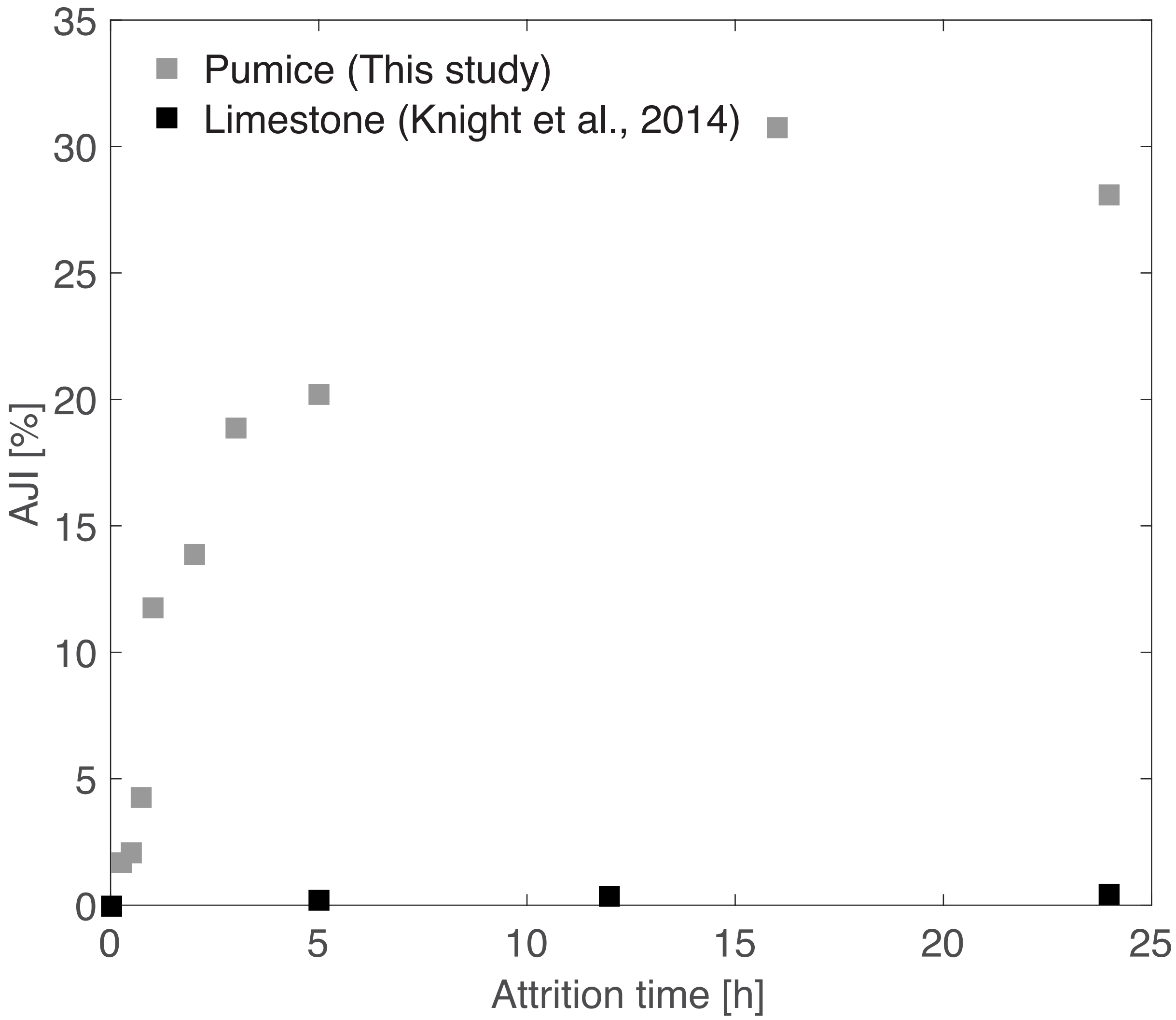

Figure 3: Jones et al., (in prep. for powder tech.)

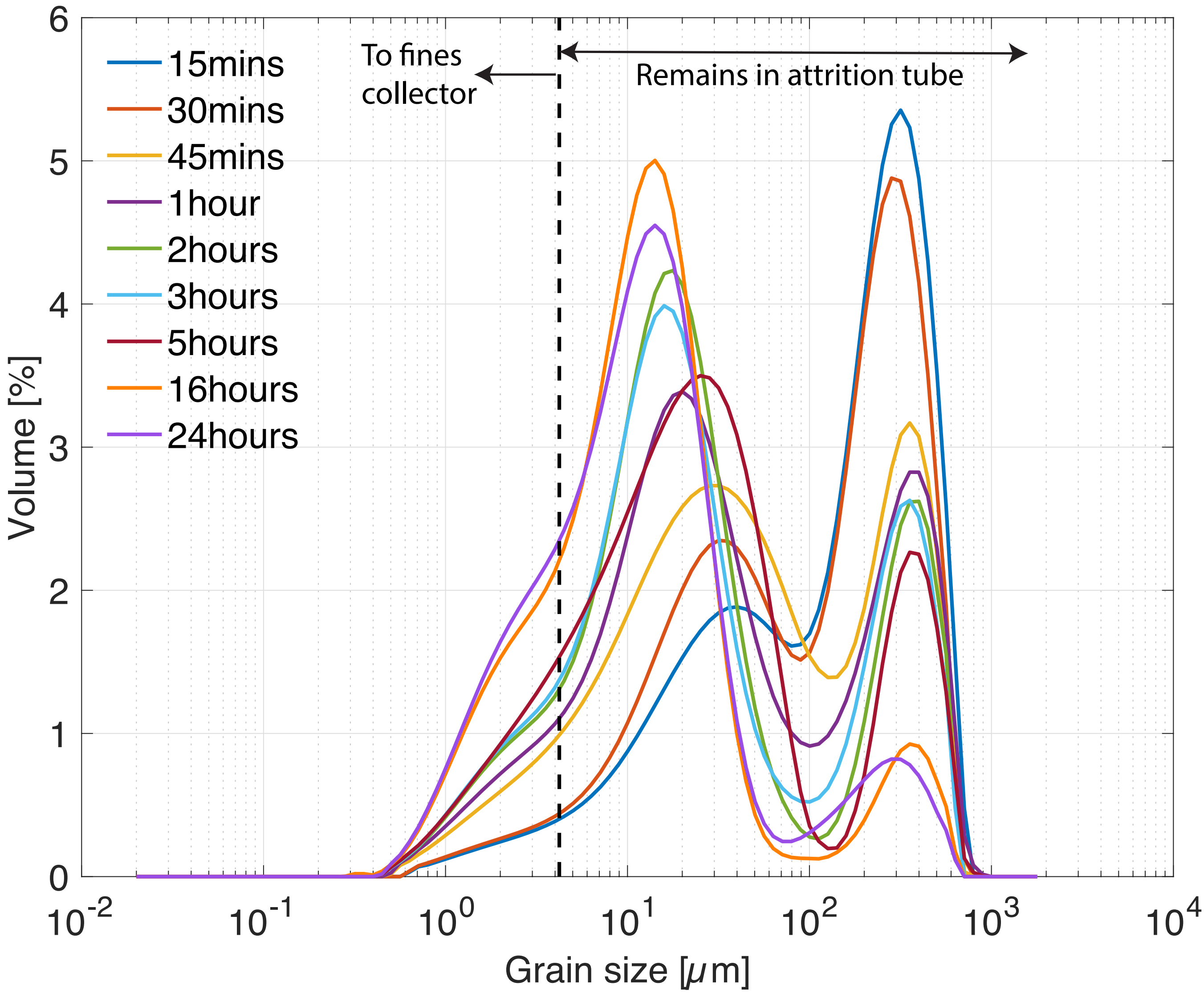

Figure 4: Jones et al., (in prep. for powder tech.)

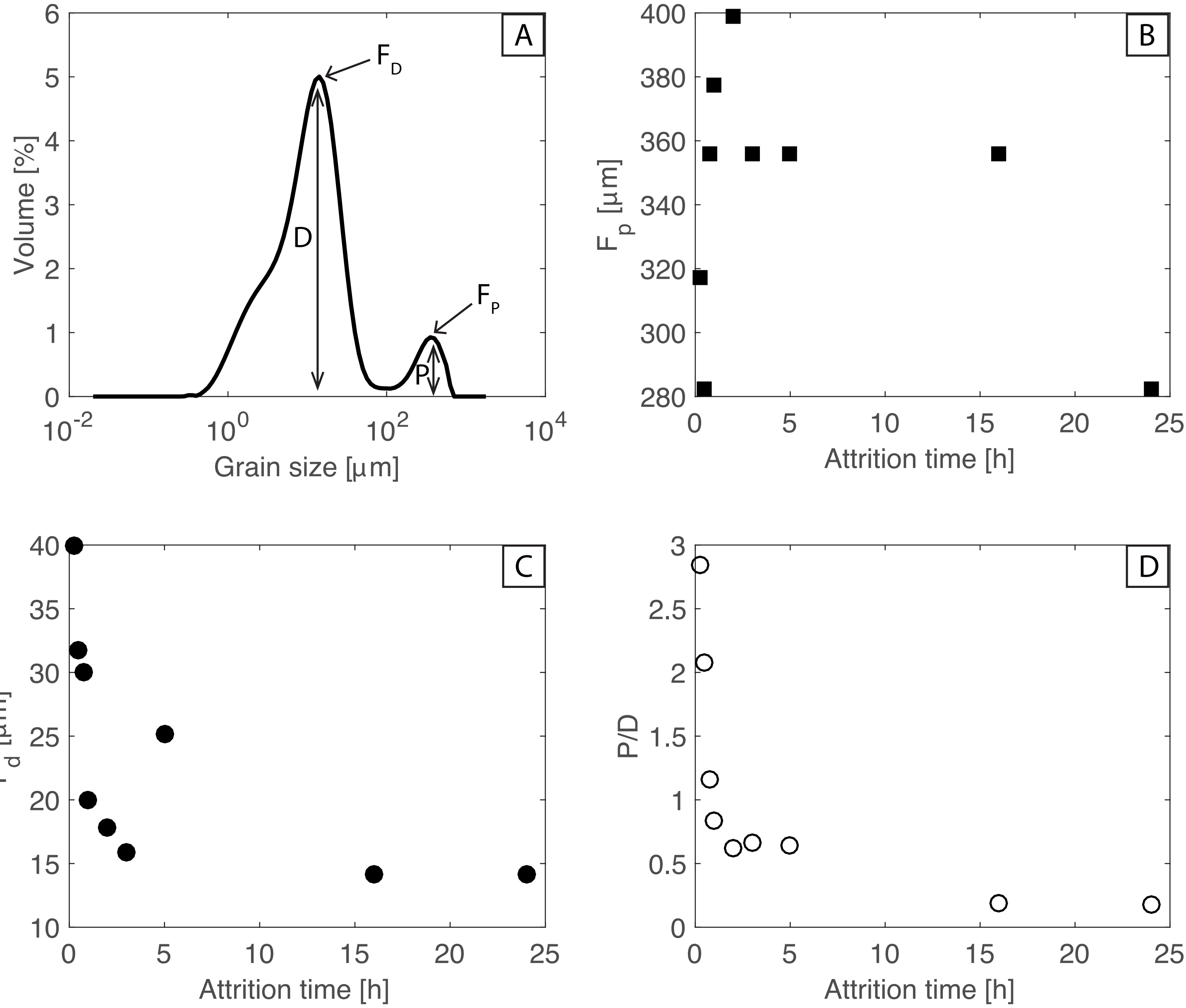

Figure 5: Jones et al., (in prep. for powder tech.)

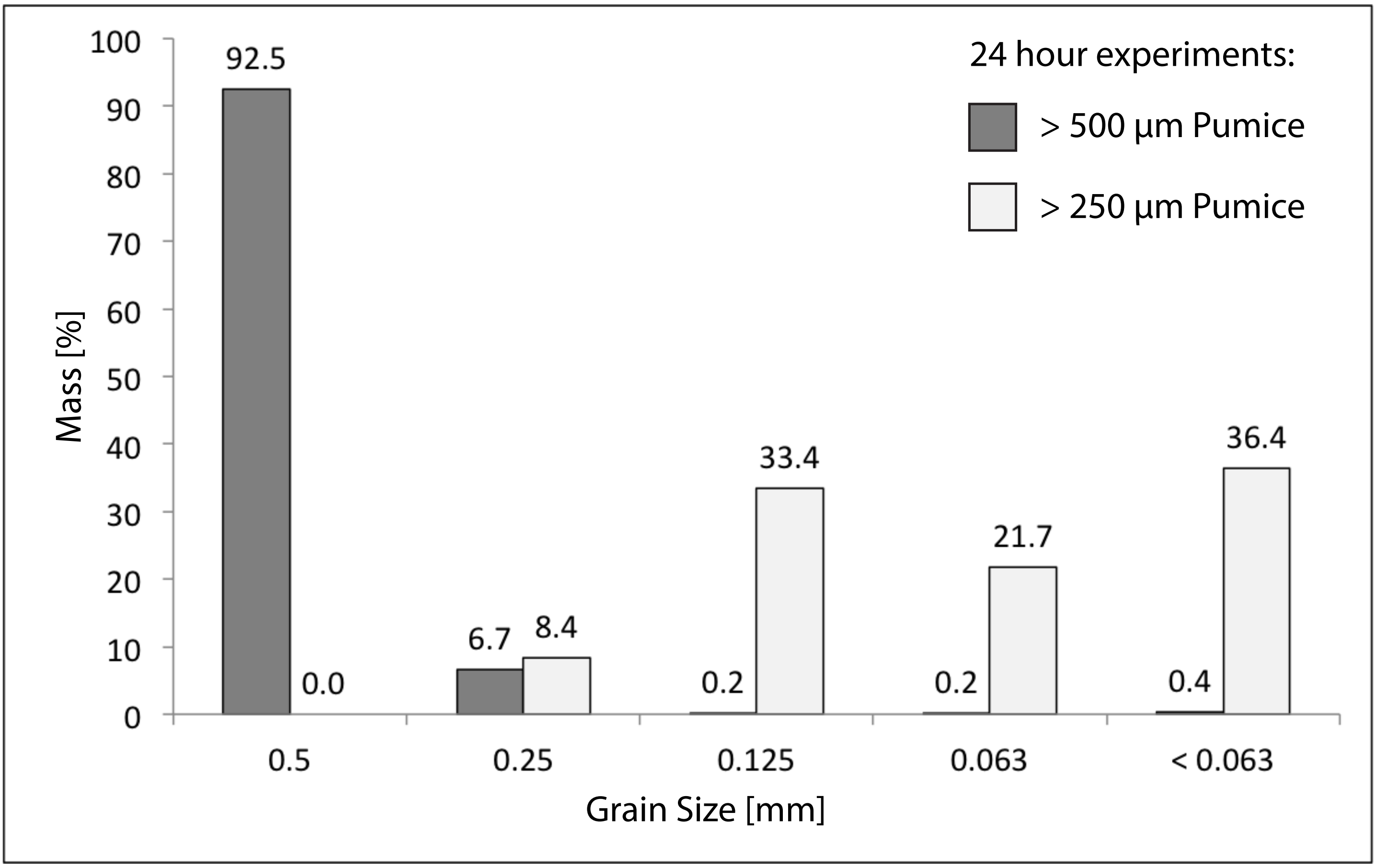

Figure 6: Jones et al., (in prep. for powder tech.)

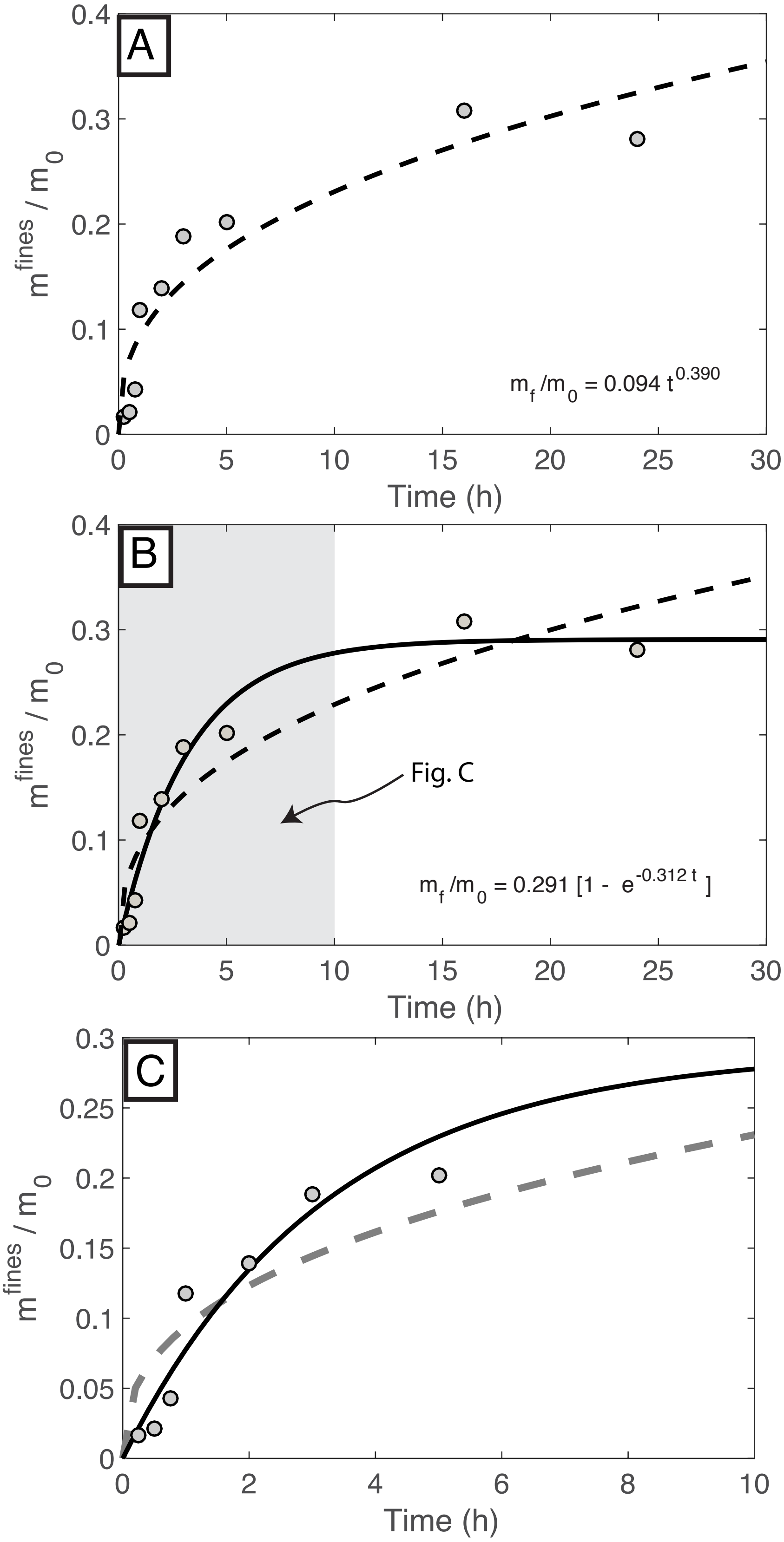

Figure 7: Jones et al., (in prep. for Powder Tech.)

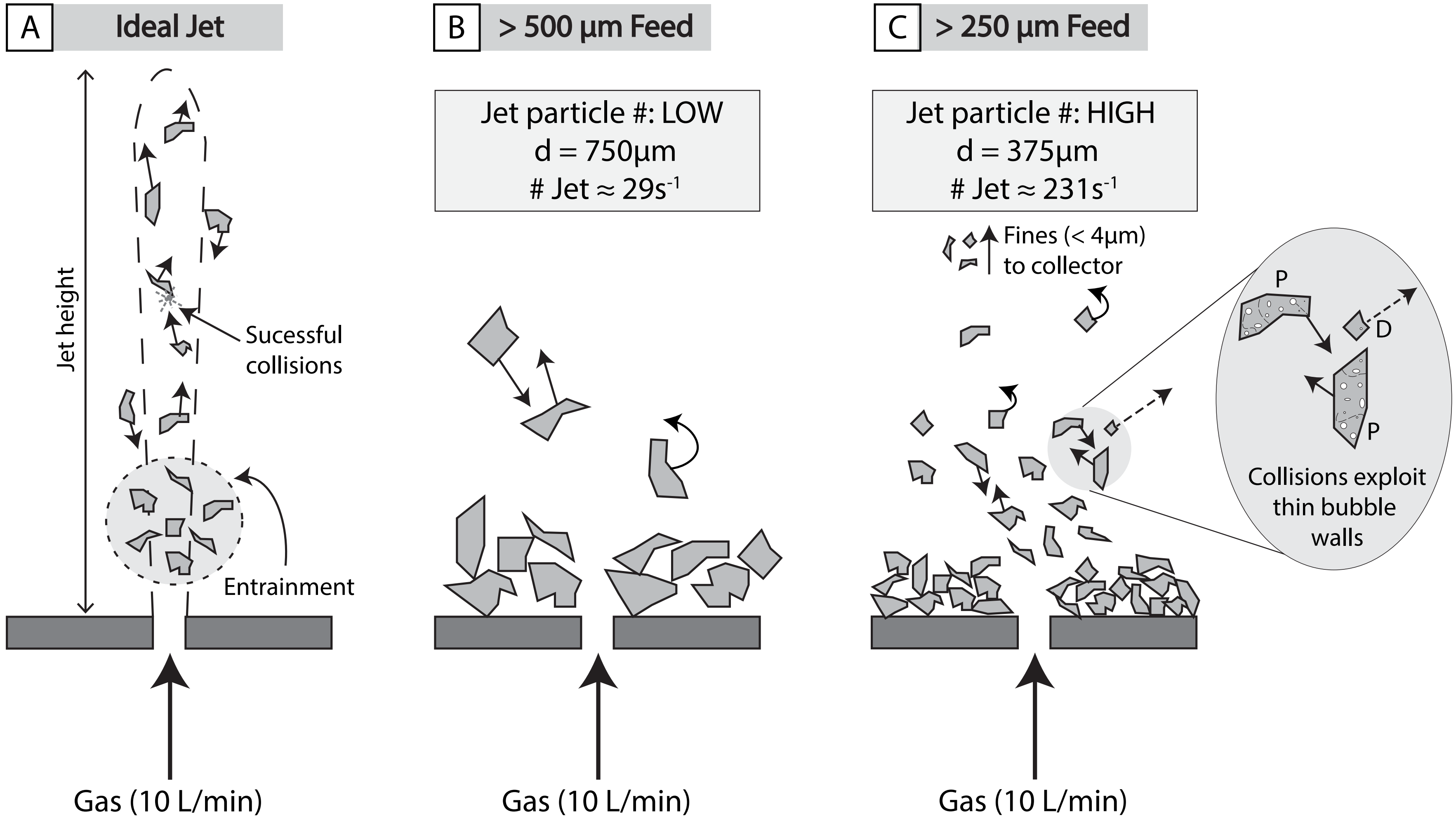

Figure 8: Jones et al., (in prep. for Powder Tech.)

Material	Duration [h]	Initial size bin [µm]	Mass [g]
MMP	0.25	250	20.0000
MMP	0.5	250	20.0000
MMP	0.75	250	20.0006
MMP	1	250	20.0001
MMP	2	250	20.0000
MMP	3	250	20.0001
MMP	5	250	20.0006
MMP	16	250	20.0001
MMP	24	250	20.0001
MMP	16	500	20.0173
MMP	24	500	20.0005

Table 1: Jones et al., (in prep. for Powder Tech.)

Duration [h]	m^{0}_{bed} [g]	m_{fines} [g]
0.25	20.0000	0.3336
0.5	20.0000	0.4196
0.75	20.0006	0.8567
1	20.0001	2.3589
2	20.0000	2.7798
3	20.0001	3.7718
5	20.0006	4.0343
16	20.0001	6.1514
24	20.0001	5.6154
16	20.0173	0.3336
24	20.0005	0.4196

Table 2: Jones et al., (in prep. for Powder Tech.)